Research Article

Biomolecular Condensation of the Human Papillomavirus E2 Master Regulator with p53: Implications in Viral Replication

Silvia Susana Borkosky [1]*, Marisol Fassolari [2], Karen Campos-León [3], Andrés Hugo Rossi [1], Mariano Salgueiro [1], Carla Antonela Pascuale [1], Ramón Peralta Martínez [1], Kevin Gaston [4] and Gonzalo de Prat Gay [1]*

*1 - **Fundación Instituto Leloir,** Instituto de Investigaciones Bioquímicas de Buenos Aires (IIBBA) - CONICET, Av. Patricias Argentinas 435, 1405 Buenos Aires, Argentina*

*2 - **Fundación para Investigaciones Biológicas Aplicadas (FIBA),** Instituto de Investigaciones en Biodiversidad y Biotecnología (INBIOTEC)-CONICET, Mar del Plata, Argentina*

*3 - **Division of Immunity and Infection,** School of Medicine, University of Birmingham, United Kingdom*

*4 - **School of Medicine,** University of Nottingham Biodiscovery Institute, Nottingham, United Kingdom*

***Correspondence to Silvia Susana Borkosky and Gonzalo de Prat Gay:** sborkosky@leloir.org.ar (S.S. Borkosky), gpg@leloir.org.ar (G. de Prat Gay) @pratgaylab (G. de Prat Gay)*

https://doi.org/10.1016/j.jmb.2022.167889

Edited by Andrew Mouland

Abstract

p53 exerts its tumour suppressor activity by modulating hundreds of genes and it can also repress viral replication. Such is the case of human papillomavirus (HPV) through targeting the E2 master regulator, but the biochemical mechanism is not known. We show that the C-terminal DNA binding domain of HPV16 E2 protein (E2C) triggers heterotypic condensation with p53 at a precise 2/1 E2C/p53 stoichiometry at the onset for demixing, yielding large regular spherical droplets that increase in size with E2C concentration. Interestingly, transfection experiments show that E2 co-localizes with p53 in the nucleus with a grainy pattern, and recruits p53 to chromatin-associated foci, a function independent of the DNA binding capacity of p53 as judged by a DNA binding impaired mutant. Depending on the length, DNA can either completely dissolve or reshape heterotypic droplets into irregular condensates containing p53, E2C, and DNA, and reminiscent of that observed linked to chromatin. We propose that p53 is a scaffold for condensation in line with its structural and functional features, in particular as a promiscuous hub that binds multiple cellular proteins. E2 appears as both client and modulator, likely based on its homodimeric DNA binding nature. Our results, in line with the known role of condensation in eukaryotic gene enhancement and silencing, point at biomolecular condensation of E2 with p53 as a means to modulate HPV gene function, strictly dependent on host cell replication and transcription machinery.

Introduction

Human papillomaviruses (HPVs) infect epithelial cells and can induce the formation of benign hyperproliferative lesions.[1] However, persistent infection with a viral subset, known to be oncogenic, can result in anogenital or oropharyngeal cancers.[1–2] HPV-associated cancers express the viral E6 and E7 oncogenes, and the products of these genes increase cell proliferation and promote cell immortalization.[3] The HPV E2 protein is the master regulator of the virus life cycle, with roles in the control of gene transcription and viral genome replication[4]. The role of E2 in transcription is well characterized,

Please cite tts article as: S.S. Borkosky, M. Fassolari, K. Campos-León, et al., Biomolecular Condensation of the Human Papillomavirus E2 Master Regulator with p53: Implications in Viral ReplicationJournal of Molecular Biology, https://doi.org/10.1016/j.jmb.2022.167889

it binds specifically to sequence motifs in the viral genome and can activate or repress transcriptional processes in a dose-dependent manner.[4–5] In this context, recruitment of many cellular transcription factors and coactivators by E2 is needed to activate viral transcription. In addition, E2 functions as a loading factor for the E1 helicase, facilitating binding of E1 to the replication origin, leading to formation of the E1-E2 replication initiation complex[6]. In later stages of replication, E2 facilitates maintenance and partitioning of the viral genome by tethering it to host chromatin.[5] The E2 proteins are around 400 amino acid polypeptides consisting of an N-terminal transactivation domain (ca. 200 amino acids) and a C-terminal DNA binding and dimerization domain (E2C, ca. 85 amino acids), separated by a non-conserved "hinge" domain. The E2C domain folds as an obligated dimeric β-barrel, consisting of 2 half-barrels each composed of 4 β-strands and 2 α-helices: one α-helix from each half-barrel acts as a DNA recognition site.[7–8]

Tumour suppressor p53 protein is a global transcription factor essential for the prevention of cell transformation and ultimately cancer progression.[9–10] The functional complexity of p53 is reflected by its structural organization, i.e., a modular domain structure, consisting of independently folded DNA-binding ($p53_{DBD}$) and tetramerization (p53 tet) domains and intrinsically disordered regions that account for about 40% of the full-length protein.[11] These disordered regions include the negatively charged N-terminal transactivation domain ($p53_{TAD}$), a short proline rich region, and the C-terminal regulatory domain ($p53_{CT}$).[11] A wide variety of stress signals are known to induce p53 activity, including viral infection.[12] In fact, the elucidation of p53 function emerged from early investigations on how DNA tumour viruses cause cancer.[13] These early studies demonstrated that proteins from three distinct tumour viruses – SV40 T-antigen, E1B-58k adenovirus protein, and HPV E6 oncoprotein, – formed complexes with p53[10,13]. Soon later, it was established that the principal role of HPV E6 was to interfere with the transcriptional activity of p53 and induce its degradation.[14] Interestingly, p53 was subsequently found at the viral replication sites of SV40, herpes simplex virus-1 (HSV-1), cytomegalovirus (CMV) and adenovirus[15–18]. Replication of HPV is carried out at replication foci, containing the viral helicase E1 and E2.5,6. These E1/E2 foci represent viral replication complexes (RCs), that recruit DNA damage response (DDR) proteins to support the synthesis of viral DNA, thus hijacking the cellular DNA repair processes for the virus own benefit.[19] E2 protein was shown to bind to p53 by pull-down assays *in vitro* and in cells[20–21]. Moreover, p53 has been shown to target E2 to inhibit HPV DNA replication and transcriptional activity, and the HPV E2 proteins can induce p53-dependent apoptosis.21,22,41 Nevertheless, there is no mechanistic or structural information on how this interaction takes place.

Liquid–liquid phase separation (LLPS) or biomolecular condensation underlies the formation of membrane-less organelles (MLOs) as a mechanism to dynamically compartmentalize the intracellular space in temporal terms.[23–25] Hydrophobic and electrostatic interactions driven by intrinsically disordered regions (IDRs) in proteins, weak multivalent interactions, modular and oligomeric structure, and nucleic acid binding proteins, all promote LLPS.[26–27] A multimutated p53 variant was shown to undergo homotypic LLPS *in vitro*, and this was proposed to regulate p53 function.[28] Another recent study showed that, under strong crowding conditions, the p53 DNA binding domain phase-separates *in vitro,* also describing GFP-p53 liquid-like condensates in the nucleus.[29] Regarding viral infections, LLPS has been demonstrated to take part in the replication factories of *Monegavirales* and other RNA viruses.[30–31] This is not surprising as MLOs, such as nucleoli and nuclear speckles, play essential roles in RNA processing, rRNA synthesis, ribosome assembly, and mRNA splicing.[32–33] By contrast, the mechanism of formation of RCs in nuclear-replicating DNA viruses, is less understood. In the last few years, growing evidence supports the hypothesis that phase-separated compartments are involved in replication of herpesviruses and adenoviruses.[34–35] Despite this, how LLPS influences the compartmentalization and organization of DNA viral processes, and whether this phenomenon is common to a wide extent of DNA virus families remain unknown. In particular, information about the maturation of RCs is lacking, especially when considering that – at least for herpesviruses – condensates appear to change their properties and components throughout infection.[34] Besides its high impact on public health, the HPV family represent a paradigmatic model of DNA tumour viruses, as they share similar strategies to achieve productive infection with other DNA viruses that replicate in the nucleus.[36] Detailed insights into mechanisms of virus-induced assemblies are paramount to understand essential aspects of their biology, and hence uncover processes that rule virus-host cell interactions.

In this work we show that the HPV E2-p53 interaction that mediates viral replication in cells is based on a direct interaction of the proteins that result in heterotypic LLPS**.** This interaction takes place through the E2 DNA binding domain and the N terminal transactivation domain of p53. E2C can modulate the condensation process to yield highly regular liquid-like droplets with a finely tuned stoichiometry. While small DNA duplexes dissolve the droplets, long DNA fragments reshape them into amorphous condensates containing both proteins and the DNA, consistent with the

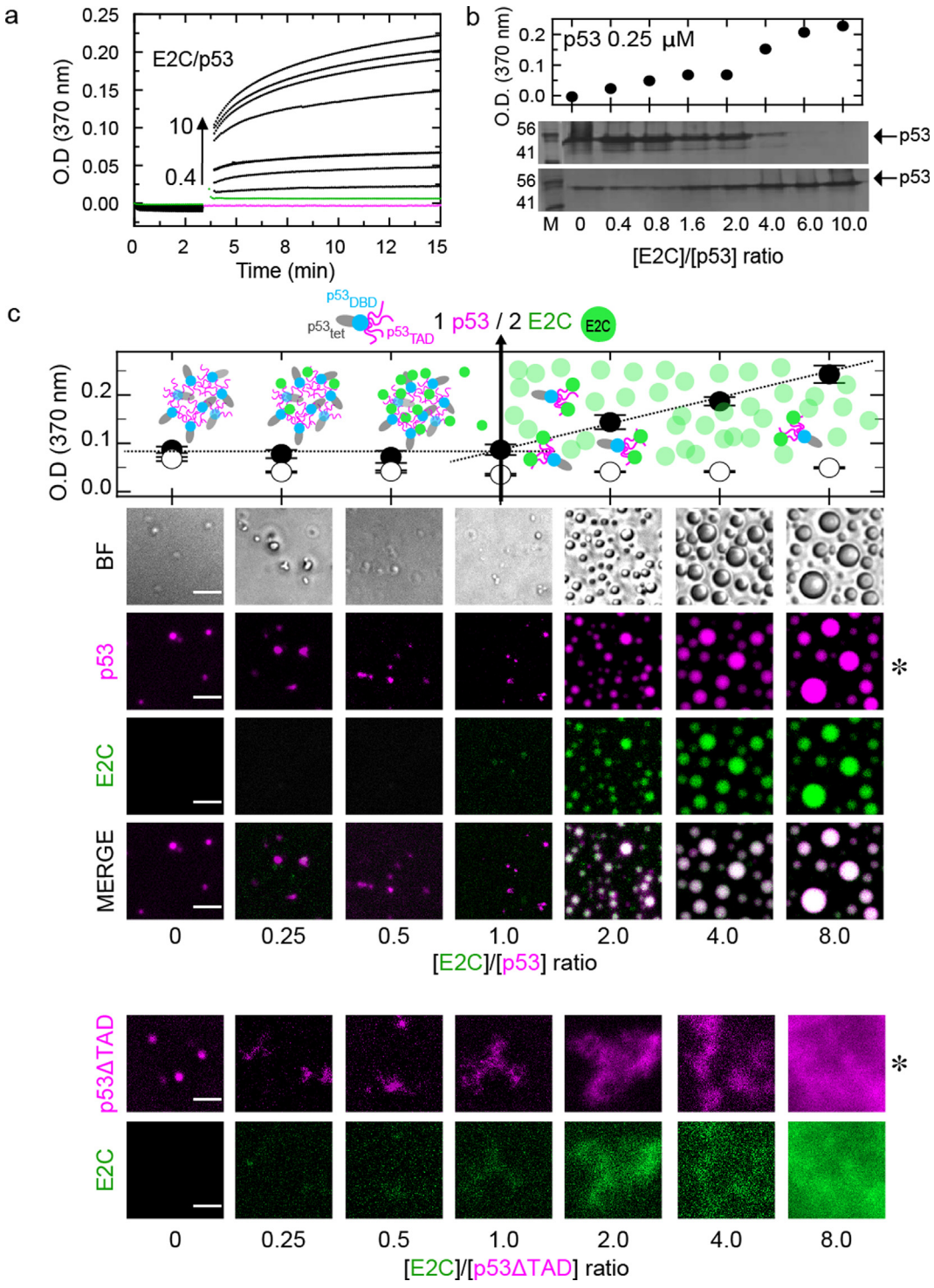
a
O.D (370 nm)
E2C/p53
10
0.4
Time (min)
b
O.D. (370 nm)
p53 0.25 μM
p53
p53
M 0 0.4 0.8 1.6 2.0 4.0 6.0 10.0
[E2C]/[p53] ratio
c
p53DBD
p53tet
p53TAD
1 p53 / 2 E2C
E2C
O.D (370 nm)
BF
p53
E2C
MERGE
0 0.25 0.5 1.0 2.0 4.0 8.0
[E2C]/[p53] ratio
p53ΔTAD
E2C
0 0.25 0.5 1.0 2.0 4.0 8.0
[E2C]/[p53ΔTAD] ratio

colocalization of both proteins at chromatin associated foci that we here describe. This work provides a biochemical basis for HPV gene modulation by p53 acting on the E2 master regulator.

Results

Interaction between p53 and HPV16 E2C leads to heterotypic droplets finely tuned by stoichiometry

Besides its main role as tumor suppressor, p53 is an important sensor of cellular stress, and has been proposed as an antiviral factor.[37–38] Indeed, among interaction with other viral proteins, p53 interacts with the C-terminal domain of E2 protein from high-risk HPVs.[20–22,39–41] Considering that the mechanism involved in the interplay between HPV E2 and p53 has not yet been elucidated, we decided to address the nature of the interaction between the two proteins, based on the initial mapping in transient transfection experiments.[21] We used the HPV16 C-terminal DNA-binding domain of E2 (E2C), and a rationally designed stability mutant of the full-length protein, previously described as pseudo wild-type p53.[42] It should be noted that p53 is a tetramer with a K_d of 50 nM[43] while E2C is an obligated dimer with a K_d of 30 nM,[44] thus, we refer to tetramer concentration for p53 and dimer concentration for E2C throughout this work. E2C-p53 interaction was followed by light scattering turbidity. When both proteins were co-incubated at different concentration ratios using a fixed p53 concentration, we observed a kinetic increase in absorbance scattering at 370 nm as a function of E2C concentration (Figure 1(a), (b)). E2C and p53 individually showed no considerable signal at 370 nm (Figure 1(a)). SDS-PAGE analysis of soluble and insoluble fractions of the samples showed a stoichiometric formation of a centrifugable material between 2/1 and 4/1 E2C/p53 ratios (Figure 1 (b)). The formation of these species upon co-incubation of both proteins prompted us to consider a phase separation process. To test this hypothesis, fixed amounts of fluorescently labelled cy5-p53 were incubated with increasing concentrations of fluorescein-labelled E2C (FITC-E2C). Within one hour, a sharp increment in turbidity matching droplet formation took place at 2/1 E2C/p53 ratio (Figure 1(c)). Complete colocalization of both proteins was observed within regular spherical droplets. Also, the size of the droplets was dependent on protein concentration (Figure 1(c)). Previous studies using multi-mutated[28] and truncated proteins[29] demonstrated that p53 undergoes *in vitro* phase separation under certain conditions. In agreement with this, samples containing p53 alone were characterized by the formation of small (1–2 μm diameter) regular droplets as judged by both fluorescence and bright field (BF) microscopy (Figure 1(c)). In control experiments, we observed that droplet formation was independent of the fluorophore used (Supplementary Figure 1(a)). Highly concentrated samples of E2C remained soluble indicating that, contrary to what has been observed with p53, E2C is unable to undergo phase separation by itself (Supplementary Figure 1(a)). After a 7-hour incubation period, the samples containing p53 alone and those with sub-stoichiometric amounts of E2C (E2C/p53 ratios of 0.25 to 1.0) evolved to less regular bead-like structures, with colocalization of both proteins (Supplementary Figure 1(b)). Based on the observed stoichiometry, further experiments were performed using a fixed E2C/p53 concentration ratio of 4/1 to ensure optimal conditions for heterotypic LLPS.

p53-E2C condensation is mediated by the N-terminal transactivation domain (TAD) of p53

As LLPS frequently involves electrostatic interactions,[45–46] we hypothesized p53-E2C condensation to be mediated by interaction between the highly positively charged E2C with the negatively charged N-terminal domain of p53 ($p53_{TAD}$). Therefore, we prepared a truncated mutant lacking the $p53_{TAD}$, and named it p53ΔTAD. We investigated whether droplet formation of this deletion mutant occurred under similar conditions as those described above for the full-length protein (Figure 1 (c)). By turbidity experiments, we observed similar values of absorbance signal for both p53 and p53ΔTAD from stoichiometric ratios up to 1.0

Figure 1. E2C-p53 interaction triggers the formation of regular heterotypic droplets. (**a**) Kinetic light scattering plot of individual samples containing 0.25 μM p53 incubated for 3 minutes, followed by addition of increasing concentrations of HPV16 E2C (Black dots). Samples with E2C/p53 ratios of 0.4, 0.8, 1.6, 2.0, 4.0, 6.0 and 10.0 were included. Control samples contained 0.25 μM p53 (Magenta dots) or 2.5 μM E2C (Green dots). (**b**) Plot of the final points of the kinetic assay from (a) (Upper panel). Soluble (Upper gel image) and insoluble (Lower gel image) fractions of the samples obtained by centrifugation and analysed by SDS-PAGE electrophoresis (Lower panel). M, molecular weight marker. (**c**) Turbidity assay monitoring absorbance at 370 nm on individual samples containing 2.5 μM cy5-p53 (Black circles) or 2.5 μM cy5-p53ΔTAD (Open circles) and increasing FITC-E2C concentrations. Blue circles correspond to $p53_{DBD}$, magenta chains to $p53_{TAD}$, grey cylinders to p53 tet domains, green circles to E2C, and light green circles to excess of E2C (Upper panel). Representative microscopy images of the samples measured in the plot and visualized after incubation for 1 hour (Lower panel). Asterisk shows the same condition for p53 vs. p53ΔTAD. BF, bright field. Scale bars = 10 μm.

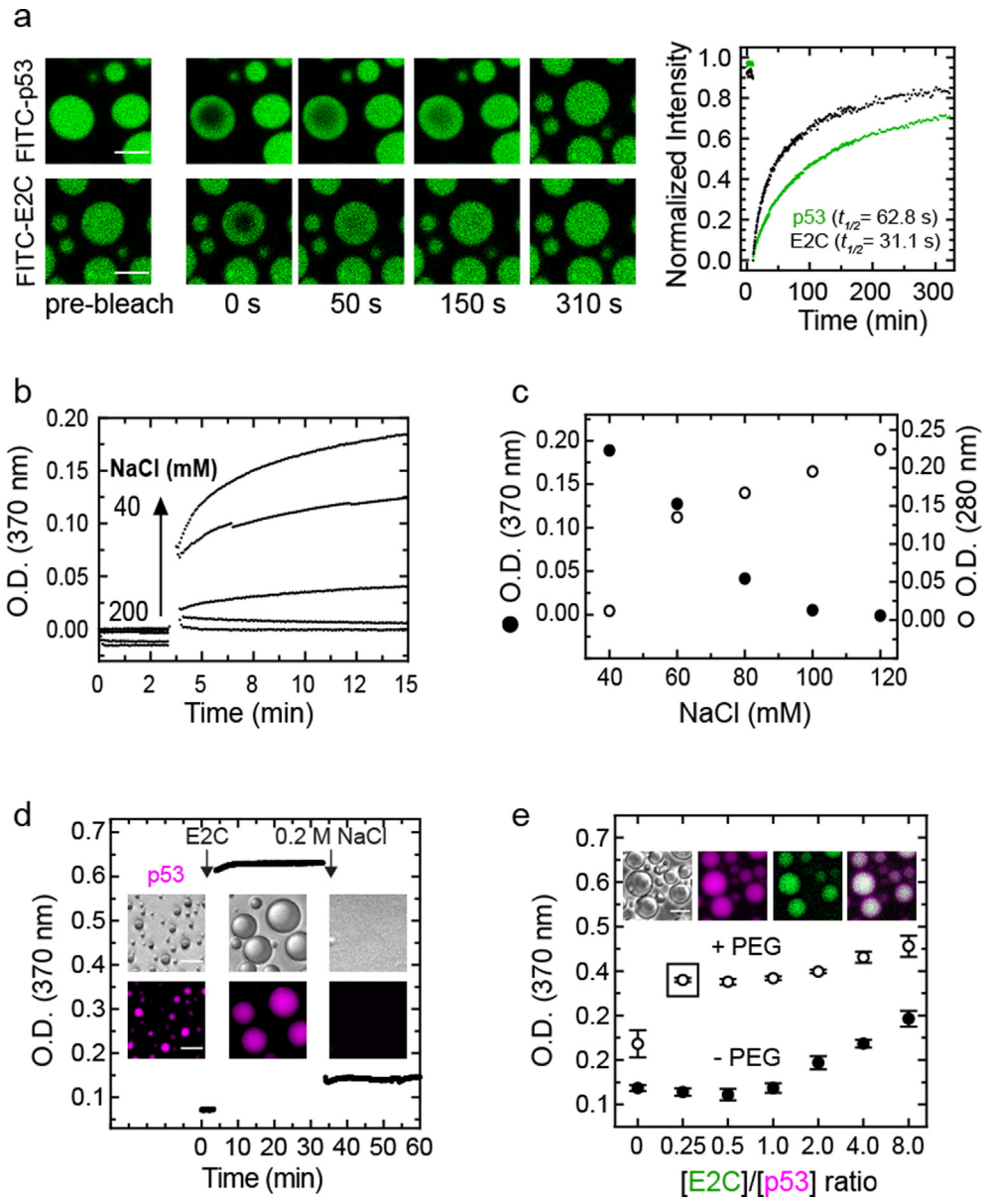

Figure 2. Material properties of E2C/p53 heterotypic LLPS. (**a**) Representative confocal microscopy images and mean plot of FRAP analysis of heterotypic spherical droplets composed of 2.5 μM FITC-p53 and 10 μM unlabelled E2C (Upper image panel and green dots on plot) or 2.5 μM unlabelled p53 and 10 μM FITC-E2C (Lower image panel and black dots on plot). Data were normalized to the average intensity of a droplet not photobleached and fitted using a double exponential function (n (p53) = 7 droplets; n (E2C) = 8 droplets). Scale bars = 5 μm. (**b**) Kinetic light scattering plot of individual samples containing pre-incubated p53, followed by addition of E2C (E2C/p53 ratio = 2.0) with NaCl concentrations ranging from 40 mM to 200 mM. (**c**) Centrifugation of the samples from (b) was followed by measurement of absorbance signal at 280 nm (Open circles), plotted in comparison to the scattering absorbance signal at 370 nm (Black circles). (**d**) Turbidity kinetic assay combined with bright field and fluorescence microscopy. Heterotypic condensation was triggered by addition of E2C to pre-formed cy5-p53 homotypic droplets and reversed by increasing the ionic strength. Scale bars = 10 μm. (**e**) Turbidity assay monitoring samples containing 2.5 μM cy5-p53 and increasing E2C concentrations with 10% PEG (Open circles) in comparison to similar samples without crowding agent (Black circles) (Same samples as in Figure 1(c)). Representative microscopy images of the samples with E2C/p53 ratio of 0.25 in presence of 10% PEG (Highlighted with box on plot). Scale bars = 10 μm.

(Figure 1(c), plot). On the other hand, at conditions with ratios above 1.0, absorbance signals showed no increase for samples containing p53ΔTAD (Figure 1(c), plot). Microscopy imaging of the samples revealed that, while p53ΔTAD was able to form homotypic droplets similar to those formed by the

full-length p53, no heterotypic droplets were observed at any of the E2C/p53ΔTAD ratios evaluated (Figure 1(c), Supplementary Figure 2). Moreover, increasing the concentration of E2C resulted in the formation of amorphous aggregates with co-localization of both proteins (Figure 1(c), Supplementary Figure 2(a)). Interestingly, both protein colocalization and size of E2C-p53ΔTAD aggregates were time-course dependent (Supplementary Figure 2(b)). Overall, these findings demonstrate that interaction between E2C and $p53_{TAD}$ is required to trigger E2C/p53 droplet-like condensates. The fact that interaction between E2C and p53ΔTAD led to aggregate formation strongly suggests that E2C interacts with other regions of p53, and requires further investigation.

Properties of the E2C/p53 condensates

The E2C/p53 droplets showed liquid-like features based on their ability to fuse upon coalescence, relaxing to regular spherical shapes in less than 10 seconds (Supplementary Figure 3(a)). To gain further insight into the material properties of the heterotypic E2C/p53 droplets we carried out fluorescence recovery after photobleaching (FRAP) analysis in separate individual experiments using FITC labelling on each protein for a more consistent comparison (Figure 2(a), Supplementary Figure 3(b)). p53 recovered 73% of the pre-bleach intensity, with a $t_{1/2}$ of 63 seconds, and E2C recovered to a similar extent (84%) but with a significantly faster recovery rate than that of p53 ($t_{1/2}$= 31 seconds) (Figure 2(a)). For each protein, a major exponential phase governed the process (Supplementary Figure 4).

Having shown that E2C/p53 droplet formation is based on interaction through the highly acidic $p53_{TAD}$, we sought to investigate the role of charge interactions by modifying the ionic strength. First, we monitored the turbidity of a mixture of E2C/p53 with increasing concentrations of NaCl, observing signal disappearance at 100 mM salt concentration (Figure 2(b)), with concomitant increase of protein soluble fraction, the latter monitored by absorbance at 280 nm (Figure 2(c)). We confirmed the complete reversibility of this ionic strength-dependent process by performing a sequential kinetic assay. For this, E2C was added to the pre-formed small p53 homotypic droplets at low salt concentration, giving rise to a pronounced increase in absorbance and the formation of the larger heterotypic droplets within the experimental deadtime (ca. 20 seconds) (Figure 2(d)). Subsequent addition of 200 mM NaCl completely reversed both the droplets and turbidity (Figure 2(d)). Next, we evaluated the effect of molecular crowding by including 10% PEG 4000 in the sample. The protein ratio onset for droplet formation in the presence of crowding agent dropped from an E2C/p53 ratio of 2.0 to 0.25 (Figure 2(e)), indicating that molecular crowding lowered the protein concentrations threshold for LLPS (Figure 2(e)).

HPV16 E2 co-localizes with p53 and recruits it to chromatin foci

To evaluate the nature of structures of p53 and HPV16 E2 in cells we made use of transfection experiments. We first addressed colocalization by expressing wild-type p53 and HPV16 GFP-tagged E2 fusion protein in Saos-2 cells, a cell line that lacks endogenous p53. In transiently transfected cells, the subcellular localization of p53 is clearly nuclear while GFP-E2 is predominantly nuclear with some cytoplasmic signal (Figure 3(a)). Co-expression revealed that the GFP-E2 protein completely colocalized with p53 in the nuclei of these cells with a homogenously dense pattern (Figure 3(a)). We next wanted to address the nature of structures formed by interaction of the two proteins within the nucleus. For this, we used C-33A cervical keratinocytes, a cell line that expresses the p53 R273C mutant, widely documented for being impaired for DNA binding.[47] This allowed us to examine an interaction between E2 and p53 in the absence of specific p53-DNA interaction, a determinant for its main and primary role in transcriptional activity. C-33A cells were transiently transfected with GFP-E2, and both proteins were monitored by immunofluorescence. Endogenous p53 R273C showed a fine grainy staining pattern homogeneously distributed in the nucleus (Figure 3(b)). A similar grainy pattern was observed when cells were transfected with GFP-E2, and the merge image shows that they indeed fully colocalized (Figure 3(b), left). Further, we performed *in situ* sub-cellular fractionation,[48] where cytoplasmic and loosely held nuclear proteins are removed and only tightly chromatin-bound proteins remain. When C-33A cells expressing GFP-E2 were subjected to this treatment, E2 and p53 colocalized to chromatin-associated condensate-like material with a coarse granular pattern (Figure 3(b), left). However, in the absence of E2, p53 R273C was not retained in the chromatin fraction (Figure 3(b), right), indicating that it is not tightly bound to chromatin.

DNA differentially modulates dissolution and reshaping of heterotypic E2C/p53 condensates

The fact that both p53 and E2 are transcriptional regulators that interact and colocalize to chromatin condensate-like foci, prompted us to investigate the effect of DNA on heterotypic condensation *in vitro*. First, we pre-formed p53-DNA complexes at increasing concentrations of a 20 bp DNA duplex containing a cognate high affinity p53 binding site, DNA_{p53}.[49] Sub-stoichiometric amounts of DNA_{p53} (DNA/p53 ratio of 0.2) caused deformation of the droplets, and bead-like aggregates were

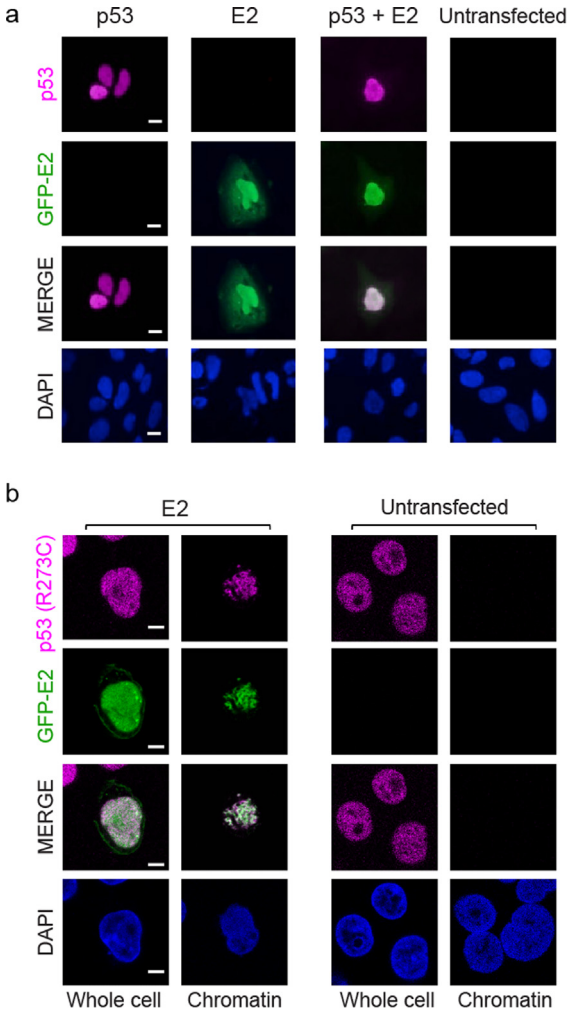

Figure 3. Colocalization of p53 and E2 in cells. (**a**) Fluorescence microscopy images of Saos-2 cells transfected with pCB6:p53 alone or in combination with pGFP HPV16 E2; protein expression was detected by immunofluoresence. GFP-E2 fusion protein and p53 were visualized with FITC and TRITC filters, respectively. DAPI staining was used to visualize the cell nuclei. Scale bars = 5 μm. (**b**) Confocal microscopy images of C-33A cells transiently transfected with pGFP E2 followed by immunofluorescence. Additionally, replicates of transfected and untransfected controls were subjected to *in situ* sub-cellular fractionation prior to immunofluorescence detection of E2 and p53 R273C, allowing for comparison between protein sub-cellular distribution within whole cells and in the chromatin fraction. GFP-E2 fusion protein and p53 R273C were visualized using FITC and TRITC filters, respectively. DAPI staining was used to visualize the cell nuclei. Scale bars = 5 μm.

observed at a DNA/p53 ratio of 0.4 (Figure 4(a)), which contained p53, E2C, and DNA, and evolved with time (Figure 4(a), Supplementary Figure 5(a) and (b)). Interestingly, when DNA_{p53} was added in stoichiometric excess (DNA/p53 ratio of 4.0), the p53-E2C droplets were dissolved without accumulation of aggregates under these conditions (Figure 4(a) and Supplementary Figure 5(a)). We have previously shown that the K_d for E2C binding to non-specific DNA is ca. 1 μM, compared to 2 nM for its specific site.[50] This means that under the micromolar concentration conditions of our experiments, E2C will also bind stoichiometrically to DNA_{p53}. In other words, although very low concentrations of DNA_{p53} will preferentially bind to p53, at higher concentrations DNA_{p53} will also bind to E2C. This suggests a small component of sequence specificity. In any case, these results strongly suggest that the DNA binding domains of both proteins are involved in stabilizing the E2C/p53 droplets.

In order to address DNA sequence specificity, we performed similar experiments using a 18 bp DNA duplex containing one E2 recognition sequence (site 35 in the HPV16 genome), named DNA_{E2C}. The E2C-DNA_{E2C} complex was pre-formed with increasing amounts of DNA, followed by addition of p53 at the reference ratio of 4/1 E2C/p53. DNA_{E2C}/E2C ratios of 0.25 (corresponding to a DNA_{E2C}/p53 ratio of 1.0) or below triggered deformation of the regular droplets (Figure 4(b), Supplementary Figure 5(c)). DNA_{E2C}/E2C ratios of 1.0 (corresponding to a DNA_{E2C}/p53 ratio of 4.0) dissolved the condensates Figure 4(b), Supplementary Figure 5(c)). Incubation of the samples at different time points demonstrated an increase in the size of the condensates and aggregates as time elapsed (Supplementary Figure 6(a)). Similarly, we evaluated the effect of an 18 bp non-specific duplex for either protein (DNA_{nonsp}) on the heterotypic droplets, by pre-incubating E2C with increasing amounts of this DNA, followed by addition of p53. The results were similar to those of the DNA_{E2C} only that the non-specific DNA led to a large amount of aggregation (Figure 4(b), Supplementary Figure 5 (d) and Supplementary Figure 6(b)).

Overall, this set of experiments indicates a small sequence specificity component for reshaping and dissolving p53-E2C LLPS droplets. A shift in stoichiometry to higher values is observed for DNA_{E2C} (Figure 4(b)) likely due to the fact that E2C is in a four fold excess of p53, the reference condition (Figure 1(c)), and more DNA is required to saturate free E2C.

Finally, we wanted to evaluate the effect of long stretches of DNA that may better approximate the DNA encountered by the proteins in the nucleus. To this end, we made use of calf thymus DNA (ctDNA), consisting of fragments of an average length of 1000 base pairs, and we represented the stoichiometry as number of 20 base pair non-specific sites along the entire fragment, approximately 50 sites (1000/20). p53-E2C LLPS droplets were pre-formed and ctDNA at increasing amounts was subsequently added, which deformed the droplets at sub-stoichiometric

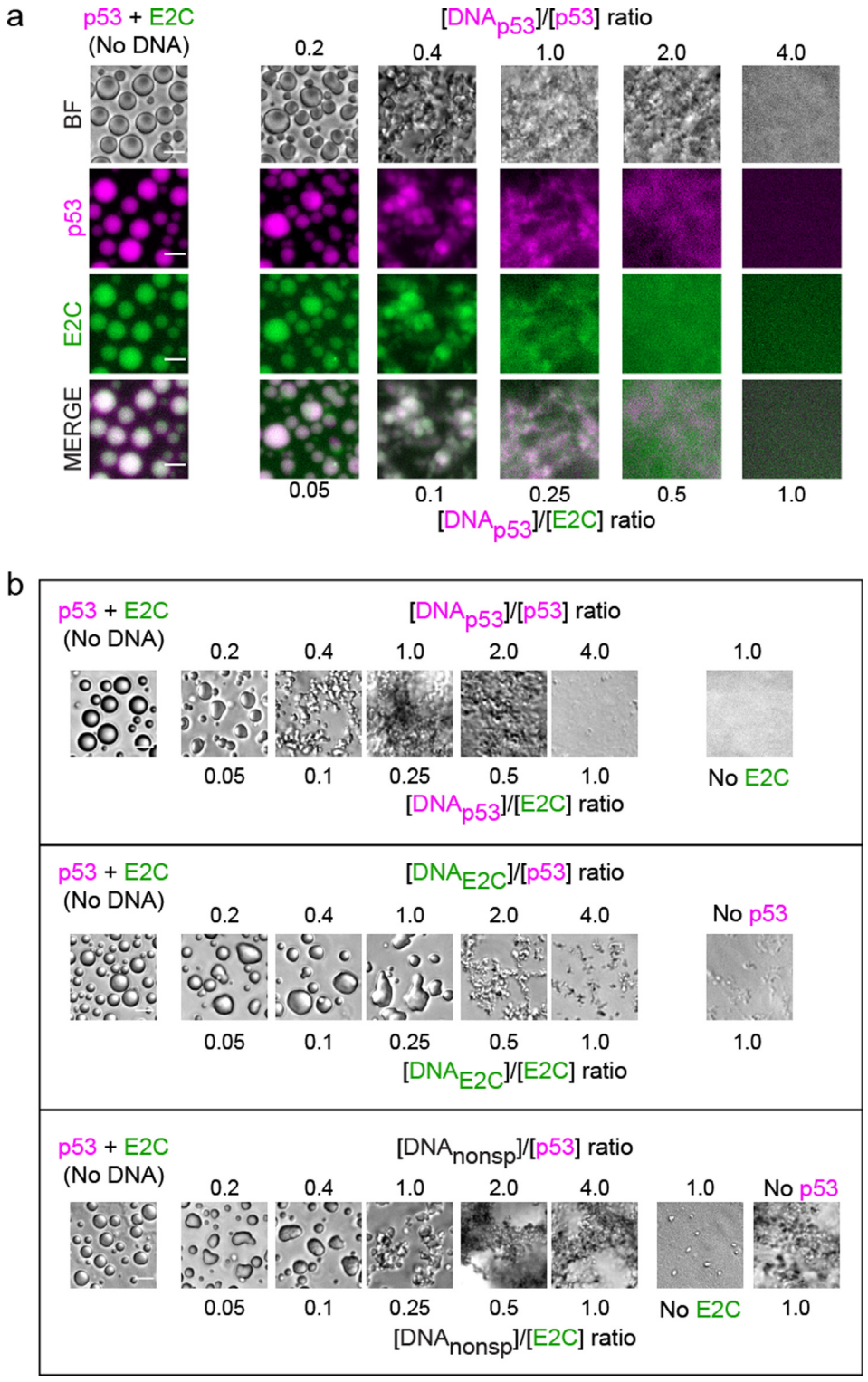

Figure 4. Effects of short specific and non-specific oligonucleotides on LLPS. (**a**) Microscopy images of samples containing increasing concentrations of DNA_{p53}, and fixed concentration of cy5-p53 and FITC-E2C (E2C/p53 ratio = 4.0) after incubation for 1 hour. Control samples contain p53 + E2C without DNA. BF, bright field. Scale bars = 10 μm. **(b)** Bright field microscopy images of samples containing fixed concentrations of cy5-p53 and FITC-E2C (E2C/p53 ratio = 4.0), and increasing concentrations of DNA_{p53} (Upper panel), DNA_{E2C} (Middle panel), and DNA_{nonsp} (Lower panel) after incubation for 30 min. Control samples consist of p53 + E2C without DNA, and p53 + DNA_{p53} (Upper panel) E2C + DNA_{E2C} (Middle panel) and p53 + DNA_{nonsp} or E2C + DNA_{nonsp} (Lower panel). Scale bars = 10 μm.

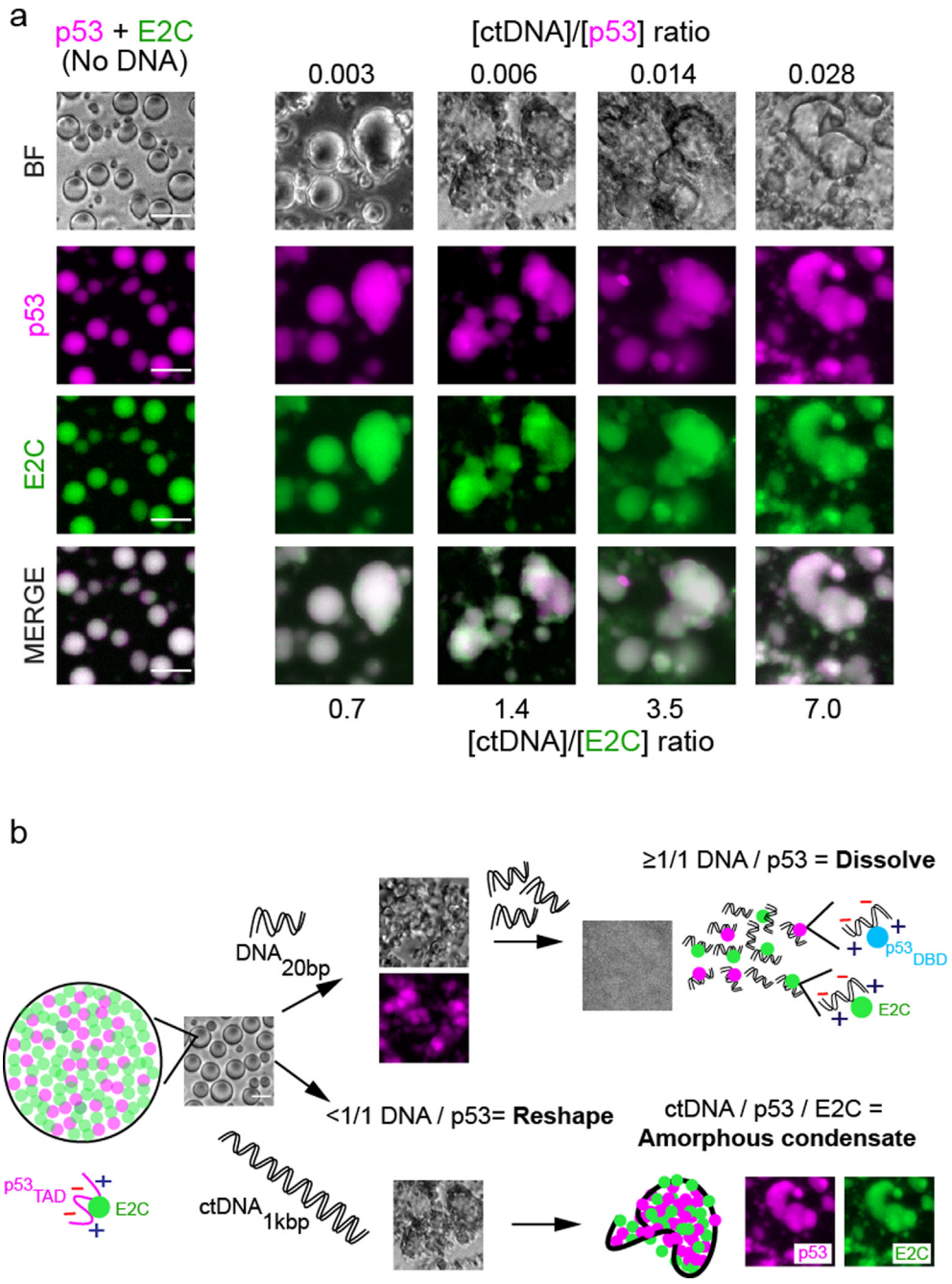

Figure 5. Effect of short DNA and long DNA on modulation of condensation. (**a**) Microscopy images of samples containing pre-formed E2C/p53 heterotypic droplets followed by addition of increasing concentrations of ctDNA. Control sample without DNA contains 2.5 μM cy5-p53 and 10 μM FITC-E2C. BF, bright field. Scale bars = 20 μm. **(b)** *Summary of the effect of short DNA and long DNA on the fate of E2C/p53 LLPS.* Short dsDNAs (∼20 bp) diffuse into the droplets where binding to $p53_{DBD}$ but also to E2C occurs. DNA competes with the negatively charged $p53_{TAD}$ for the DNA binding sites of both proteins. Gradual reshaping and dissolution of the droplets occur as a function of DNA_{20bp} concentration. Addition of the ∼ 1kbp calf thymus DNA fragment ($ctDNA_{1kbp}$) triggers the remodel of the E2C/p53 droplets into anomalous irregular condensates, which are neither droplets nor amorphous aggregates. p53 is represented as magenta circles, E2C as green circles, short and long DNAs in black.

amounts (Figure 5(a)). Higher DNA/E2C-p53 ratios led to condensation-coalescence of the initial heterotypic droplets into much larger irregular droplets containing both proteins, which ultimately evolved into larger albeit irregular condensates at longer incubation periods (Figure 5(a), Supplementary Figure 6(c)). Figure 5(b) shows a proposed model for the modulatory effect of DNA on the p53-E2C droplets.

Discussion

In this work we showed that HPV16 E2 interacts with p53 through biomolecular condensation evidenced by the formation of highly regular spherical droplets that increase in size with increased concentrations of E2C, with complete colocalization of both proteins. The onset of droplet formation is at an E2C/p53 ratio of 2.0, it takes place in the absence of added crowder, and is inhibited by ionic strength. We also, demonstrated that heterotypic droplet formation requires the interaction of E2C with $p53_{TAD}$, further supporting the role of electrostatic interactions in the condensates. FRAP experiments indicate that both p53 and E2C display dynamic properties within the droplets, with a large percent of recovery and two distinguishable rate components, which we initially ascribe to at least two populations of conformers. Interestingly, the faster recovery of E2C compared to p53 (Figure 2(a)) supports the participation of E2C as client protein which, although it is unable to undergo LLPS by itself, may form weak self-interactions and diffuse more freely within the dense phase[23]. Irrespective of this, the marked effect on droplet size increase along with E2C concentration increment is indicative of a condensate modulatory activity of the HPV master regulator.[51–53] A role as both client and modulator can thus be ascribed to the multivalent dimeric nature, DNA binding, and ionic interaction capacities of E2C. Figure 6(a) summarizes the current hypothetical model for the heterotypic condensation of p53 and E2C and proposes functional implications.

Both p53 and E2 are transcription factors that operate within the nucleus where DNA is omnipresent. In this confined environment, tight-specific as well as non-specific DNA binding is expected**.** DNA duplexes containing specific binding sites for p53 and E2C, and a DNA duplex of unspecific sequence reshaped and dissolved the E2C/p53 droplets. Excess of specific or non-specific DNA duplexes will bind E2C and p53, causing dissolution of the droplets. We conclude that the sequence specificity component at the micromolar concentrations required for LLPS is not significant. We propose that a progressive change in the material properties of the condensates takes place upon diffusion of short dsDNA (~20 bp) into the condensate, starting with deformation of the droplets, followed by an intermediate stage of reshaping of the condensates by disrupting the network of weak interactions, eventually, leading to dissolution (Figure 5(b)). A similar situation appears to take place with the long ctDNA fragment, but the reshaping does not lead to dissolution but to the formation of large irregularly shaped condensates resulting from the coalescence of the heterotypic droplets (Figure 5(b)). These heterotypic condensates are definitely not amorphous aggregates or precipitates and are compatible with the condensed material observed in the chromatin fraction in the cells where E2 and p53 colocalize (Figure 3(b)). In this model, interaction of E2 with a p53 mutant impaired for DNA binding, resulted in re-localization of this mutant to the chromatin fraction**,** indicating that the interaction of p53 with E2 could take place in the absence of p53 transcriptional activity. Considering that our study did not explore E2C/p53 LLPS in HPV replication models, we are aware that these complex interactions need to be experimentally examined in the context of HPV infection.

Biomolecular condensation is revolutionizing our understanding of intracellular compartmentalization of biochemical reactions and this phenomenon extends to the viral world, in particular to replication and transcription[30–31,54–55]. Emerging strategies common to eukaryotic gene function involve the formation of transcription factories through the assembly of phase-separated condensates as super-enhancers or repressors[56]. Likewise, there is evidence that liquid-like DNA viral replication compartments might impact on the virus-host interaction landscape[34–35,57–58]. In this context, phase separation on proteins from several dsDNA viruses, including HSV-1, Epstein-Barr virus (EBV), Kaposi's sarcoma-associated herpesvirus (KSHV), CMV, and human adenovirus (HAdV) was recently demonstrated[56,58–61]. Intriguingly, the KSHV latency associated nuclear antigen (LANA) and EBV nuclear antigen 1 (EBNA1) share functional features and noticeably, folding topologies with HPV E2[62]. Interestingly, LANA nuclear bodies (LANA-NBs) which are highly stable during latency showed partial dynamic structural properties involving phase separation condensates[61]. Moreover, LANA was shown to interact and trigger degradation of p53[63]. E1/E2 foci represent viral replication factories and recruit DDR proteins including phosphorylated p53 at serine 15[64–65]. Also, upon early infection, the capsid protein L2 interacts with E2 and recruits it to PML-NBs, and this could be important for initiation of viral replication and transcription[66]. Recently, it has been shown that the DDR component 53BP1 forms phase-separated compartments that are enriched in p53.[67] We hypothesize that a plausible mechanism for p53-mediated inhibition of HPV replication and transcription takes place through sequestration of E2 into highly stable heterotypic condensates that we observed in cells (Proposed model in Figure 6(b)). The E1 viral helicase is likely to be a functional and physical part of the condensate; especially considering that spherical E1/E2 replication foci have been widely documented.[5,64–65] In the environment of initial HPV replication, E1 interacts with the N-terminal domain of E2 (E2N). p53 could disrupt the interaction of E2C with DNA recruiting then E2/E1 into the condensate. Besides repressing HPV replica-

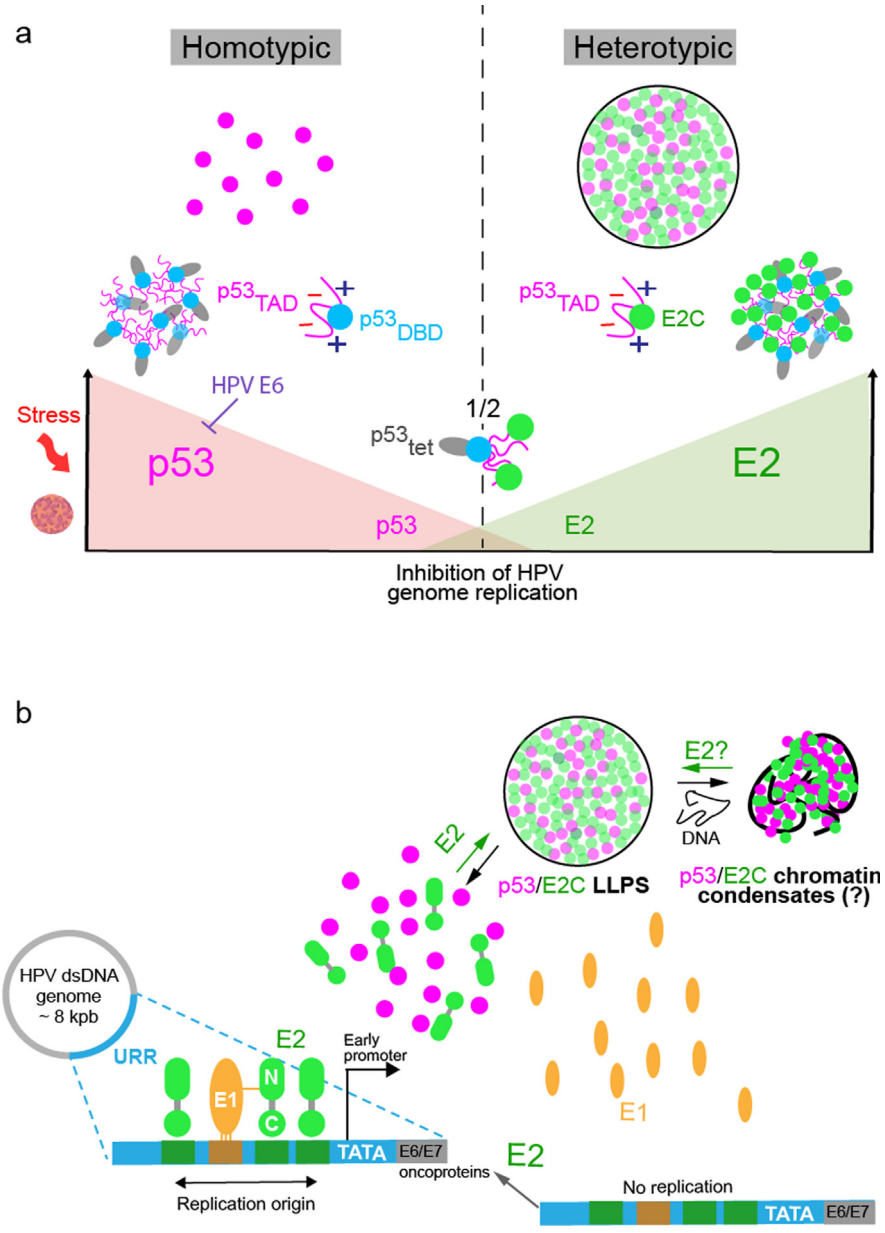

Figure 6. Proposed integrative scheme for E2C/p53 LLPS and modulation of HPV replication. (a) Interaction *between HPV E2 and p53 in the context of LLPS.* p53 levels can be elevated by the stress signal inflicted by HPV infection. p53 can inhibit viral replication but as the viral oncoprotein E6 is expressed, the latter targets p53 for proteasomal degradation. p53 can undergo homotypic LLPS and, through interaction with HPV E2, heterotypic LLPS. Blue circles correspond to $p53_{DBD}$, magenta chains to $p53_{TAD}$, grey cylinders to p53 tet domain, and green circles to E2C. (b) *Model scheme of HPV genome replication inhibition by p53.* HPV genome replication origin requires the E1 helicase which is recruited to its DNA binding site by E2 bound to adjacent high affinity binding sites, located within the upstream regulatory region (URR). Excess of p53 – product of HPV infection-induced stress – interferes with E2 binding to DNA, sequestering E2 (and perhaps E1) into condensates with consequent impairment in viral replication and transcription. As E2 levels increase the process may potentially be reverted and gene function restored.

tion, diffusion of p53 into replication compartments could be beneficial for the virus. In this context, the recruitment of p53 and perhaps other DDR factors by E2 into a condensate may also serve to hijack cellular DNA repair mechanisms to achieve accurate viral replication.[19] Moreover, a very recent study showed that disruption of p53-HPV16 E2 interaction attenuates cell growth and blocks the viral life cycle.[40]

Given p53's features, its ability to undergo spontaneous LLPS is not surprising. These include modularity, oligomerization, nucleic acid

binding, IDRs, charge distribution, and regulation by posttranslational modifications.[68–69] On the other hand, HPV E2 has been documented as a promiscuous binder.[4] This might explain its apparent role in the heterotypic condensate as client, with otherwise condensate modulatory properties. While p53 has been widely studied in HPV oncogenesis as the main target of the E6 oncoprotein, much less is known about the role of p53 during HPV infection. Further studies will aim to investigate this phenomenon in viral replication models and help identifying other viral and cellular components associated to E2C/p53 condensates.

Materials and Methods

Cloning

Specific primers were designed to generate p53ΔTAD, a truncated variant of p53 lacking the N-terminal transactivation domain ($p53_{TAD}$). The PCR product was digested with BamHI and EcoRI enzymes, purified and inserted into a modified pRSETa vector in frame with an N terminal fusion 6xHis/lipoamyl domain/TEV protease cleavage sequence. Sequencing the entire coding region and flanking sequences confirmed the truncation of the protein.

Expression and purification of recombinant proteins

The HPV16 E2 C-terminal domain (E2C) was expressed in *Escherichia coli* BL21(DE3) and purified as described previously.[50,70] The pET24a plasmid containing the sequence of a stable mutant of full-length p53 with the following mutation in the $p53_{DBD}$: M133L/V203A/N239Y/N268D[42] was a kind gift from Alan Fersht. These mutations conserve the functional and conformational properties of wild-type p53, allowing increased levels of expression and sample stability. Therefore, it is considered as pseudo wild-type p53 protein and will be referred as p53 throughout the text. p53 and p53ΔTAD were expressed in *Escherichia coli* C41 and purified by using standard His-tag purification protocols, followed by tobacco etch virus (TEV) protease digestion and heparin affinity chromatography. The final purification step was size exclusion chromatography (SEC) using Superdex-200 column (Cytiva). Conformation of p53 and p53ΔTAD was confirmed by estimating the hydrodynamic radius by dynamic light scattering (DLS). Protein concentration was determined by UV light absorbance at 280 nm using the protein molar extinction coefficients and confirmed by Bradford assay. Purified proteins were stored as at −80 °C after snap freezing in liquid nitrogen and aliquoted in fixed volumes to avoid repetitive thaw-freezing. Far-UV circular dichroism and fluorescence spectra, and SDS-PAGE were performed to confirm the quality and purity of the proteins, respectively.

Fluorescent labelling

p53 and E2C proteins were labelled with fluorescein isothiocyanate (FITC) (Sigma-Aldrich), adapting the manufacturer's protocol to obtain sub-stochiometric labelling, enough to visualize the samples by fluorescence and confocal microscopy. A p53/FITC ratio of 2 and a E2C/FITC ratio of 6 were used. Reactions were carried out at 4 °C overnight in sodium phosphate buffer 50 mM, NaCl 0.3 M and 1 mM DTT, pH 7.0. The reactions were stopped using 50 mM Tris-HCl pH 8.0 and excess of FITC was removed by desalting PD10 columns (Cytiva) eluting each protein with its corresponding stock buffer. A similar procedure was carried out for labelling p53, p53ΔTAD, and E2C with cy5 NHS (Lumiprobe) using a protein/cy5 ratio of 2. These protocols yielded proteins stocks labelled with 10% – 20% fluorescent dye.

DNAs

Double-stranded 26 bp oligonucleotides containing p53 consensus sequence[49] were prepared as follows: single-stranded oligonucleotides were purchased, HPLC purified, from Integrated DNA Technologies (Coralville, IA). DNA_{p53}A: 5' AGC TT *AG*AC*ATGCCT AGACATGCCT* A 3'' and DNA_{p53}B: 5' AGC TT *AGGCATGTCT AGG-CATG*T*CT* A 3'' (Recognition sequences are italicized). Single-stranded oligonucleotide concentration was calculated using the molar extinction coefficient obtained from the nucleotide composition. Annealing was performed as described previously.[50] This yielded double-stranded oligonucleotide termed DNA_{p53}, and no detectable single-stranded oligonucleotide was judged by PAGE. A similar procedure was followed to anneal the double stranded 18 bp oligonucleotides containing one E2 recognition sequence (site 35 in the HPV16 genome): DNA_{E2C} A: 5′ GTA *ACCG* AAAT *CGGT* TGA 3′and DNA_{E2C} B: 5′TCA *ACCG* ATTT *CGGT* TAC 3′ (Recognition sequences are italicized). A double-stranded oligonucleotide containing a randomized E2 binding site with the same nucleotide composition was used as non-specific DNA, and was composed of DNA_{nonsp} A: 5′ ACA TGG ACC TGT CAA GTA 3' and DNA_{nonsp} B: 5′ TAC TTG ACA GGT CCA TGT 3'.

Calf thymus DNA (ctDNA) (Sigma-Aldrich) was dissolved following the manufacturer's instructions to obtain a 1 mg/ml stock solution. ctDNA quantification was confirmed by nanodrop (Thermo Scientific) and quality was assessed by agarose gel electrophoresis.

Light scattering kinetic measurements

Complexes formed by E2C/p53 condensation were recorded in a Jasco UV spectrophotometer

by following scattering signals at 370 nm. Measurements were performed in 50 mM Tris-HCl, 40 mM – 200 mM NaCl (depending on the condition), and 1 mM DTT, pH 7.0. Measurements were conducted in different tubes containing a fixed p53 concentration (between 0.25 μM and 1 μM) and varying E2C concentrations. The 280 nm absorbance of soluble fractions was measured after centrifugation of the samples. This was done in the same apparatus. Then, the pellet fraction and soluble fraction (precipitated with TCA) were analysed by SDS–PAGE.

Turbidity assays

Protein samples were prepared in 50 mM Tris-HCl buffer, 40 mM NaCl, and 1 mM DTT, pH 7.0 or 50 mM Tris-HCl buffer, 150 mM NaCl, 1 mM DTT, and 10% PEG 4000, pH 7.0, in a total volume of 100 μl. The samples were incubated at room temperature for 15 min, and absorbance at 370 nm was measured using a Beckman Coulter DTX 880 multimode detector. All the conditions were measured in 96-well plates (Corning®, Flat bottom, non-binding surface). Each turbidity assay was reproduced in triplicate.

Bright field microscopy and fluorescence microscopy

Analyses of homotypic p53 LLPS and heterotypic p53/E2C LLPS were performed using bright field and florescence microscopy under varying conditions, including concentration, ionic strength, and molecular crowding. Samples were prepared at room temperature using 0.3 μM of labeled protein within the bulk of unlabeled materials and loaded into 96-well plates (Corning®, Flat bottom, non-binding surface). Sample buffer consisted of 50 mM Tris-HCl buffer, 40 mM NaCl and 1 mM DTT, pH 7.0. When molecular crowding conditions were needed, sample buffer consisted in 50 mM Tris-HCl buffer, 150 mM NaCl, 1 mM DTT and 10% PEG, pH 7.0. For fluorescence analysis, the samples were excited with LED light at 475 nm for FITC or 630 nm for cy5. The images were acquired using an inverted Axio Observer 3 microscope (Carl Zeiss) with an LD A-Plan 40x/0.55 Ph2 objective, Colibri 7 LED illumination system and a 90 HE LED filter set with BP 385/30–469/38–555/30–631/33 nm for excitation, QBS 405 + 493 + 575 + 653 nm as beam splitter and QBP 425/30 + 514/30 + 592/25 + 709/100 nm for emission. Acquired images were 1388 × 1038 pixels, with 0.233 μm × 0.233 μm pixel size, 12-bit and cropped to 150 × 150, 200 × 200, 300 × 300, or 500x 500 pixels for display. Images were processed using Fiji (A distribution package of the ImageJ software, USA).

Fluorescence recovery after photobleaching

Samples were prepared and imaged using Nunc Lab-Tek Chambered Coverglass (ThermoFisher Scientific Inc) – pre-coated with Pluronic F-127 (Sigma-Aldrich) – at room temperature, with 0.3 μM FITC-labelled samples within the total of protein concentration. Fluorescence recovery after photobleaching (FRAP) experiments were performed using a confocal laser scanning microscope (Zeiss LSM 880 Airyscan) with a C Plan-Apochromat 63x/1,4 Oil DIC M27 objective, 488 nm Argon Laser and QUASAR detector at 495–571 nm. A circular region of interest (ROI) (diameter ∼ 1 μm) was bleached using 90% laser power. Droplets of an approximate diameter of 4.5 μm were selected for heterotypic condensates (7–8n). Fluorescence intensity changes were recorded for three different ROIs (bleached droplet, reference droplet, and background) over 300 frames (350 sec), Including 10 frames before bleaching. Acquired images were 196 × 196 pixels, with 0.09 μm × 0.09 μm pixel size, 16-bit, 3 slides with 0.8 μm of section and 1.35 μsec pixel dwell. Fluorescence intensities from bleached ROIs were corrected for photofading and normalized to the bleaching depth as described.[71] Fluorescence recovery data were evaluated using the FIJI ImageJ software. Data was fit to the single exponential recovery function $y = A \times \exp(-k \times t)$ using profit 7.0.18 Quantum Soft. To improve the goodness of the fit, two-exponential fit $y = A1 \times \exp(-k1 \times t) + A2 \times \exp(-k2 \times t)$ was also used, where A and k are fitting parameters. Half time of recovery ($t_{1/2}$) was obtained graphically for the latter.

Cell culture and transient transfection

All cell lines were obtained from the ATCC. C-33A cells were maintained in Dulbecco's Modified Eagle's Medium (DMEM) (SIGMA) supplemented with 10% FBS and penicillin–streptomycin (100 units/ml and 100 μg/ml respectively) at 37 °C in 5% CO_2. Saos-2 cells were maintained as above but in the presence of 2 mM L-glutamine. C-33A cells were transiently transfected using FuGENE 6 (Roche) following the manufacturer's protocol. Saos-2 cells were transiently transfected using GeneJuice (Merck/Novagen).

Antibodies

The following antibodies were used: rabbit polyclonal Lamin A/C (H-110 Santa Cruz), mouse monoclonal α-Tubulin (Santa Cruz), rabbit polyclonal p53 (FL-393 Santa Cruz). Goat anti-rabbit IgG-TRITC (Sigma-Aldrich) was used as secondary antibody.

In situ subcellular fractionation

Cells growing on coverslips were washed twice with 1X PBS before cytoplasmic and loosely held

nuclear proteins were removed using 200 μl of CSK I buffer (10 mM PIPES, 300 mM sucrose, 100 mM NaCl, 3 mM $MgCl_2$, 1 mM EGTA pH 8.0 containing 1% (v/v) Triton X-100) for 1 min at 4 °C. The coverslips were washed twice with ice cold 1X PBS and the chromatin fixed using 4% formaldehyde for 20 min at 4 °C. α-tubulin and lamin A/C were visualized to confirm protein extraction.

Immunofluorescence

Cells growing on coverslips were washed twice with 1X PBS and fixed in 4% formaldehyde at 20 °C for 30 min followed by 3 washes with 1X PBS. After fixation, cells were permeabilized by incubation with 0.2% Triton X-100 on ice for 15 min and washed twice with 1X PBS. To reduce background staining the cells were incubated with 3% BSA at 20 °C for 20 min and washed twice with 1X PBS. The cells were incubated with primary antibody at 4 °C for 1 hour and washed twice with 1X PBS and then incubated in the dark with secondary antibody at 22 °C for 1 hour and washed twice with 1X PBS. Coverslips were mounted onto glass slides using VectaShield Mounting Medium with DAPI (Vector) and visualized by fluorescence or confocal microscopy.

Cell imaging

Cell imaging was performed using a Leica DM IRBE inverted epi-fluorescent microscope fitted with DAPI, FITC and TRITC filter sets, and a 40x objective along with the Leica IM50 Version 1.20 software (Leica) for fluorescence microscopy. A Leica DM IRBE inverted confocal microscope with a 63x objective and a TCS-NT4 software (Leica) was used for confocal microscopy. The confocal images were obtained as slices representing three averaged scans. GFP was visualized using a 488/514 nm Ar/ArKr laser (green channel), whereas TRITC was observed with a 543/594 nm HeNe laser (red channel). DNA staining was visualized at 395/405 nm (blue channel).

CRediT authorship contribution statement

Silvia Susana Borkosky: Conceptualization, Methodology, Investigation, Formal analysis, Writing – original draft, Supervision, Visualization. **Marisol Fassolari:** Investigation. **Karen Campos-León:** Investigation. **Andrés Hugo Rossi:** Methodology, Investigation. **Mariano Salgueiro:** . **Carla Antonela Pascuale:** Investigation. **Ramón Peralta Martínez:** Investigation. **Kevin Gaston:** Methodology. **Gonzalo de Prat Gay:** Conceptualization, Writing – original draft, Supervision, Visualization, Project administration, Funding acquisition.

Acknowledgments

We thank Alan Fersht for full-length p53QM expression vector. We thank Ignacio Sánchez for helpful discussions. This work was funded by ANPCyT (PICT 2019-03295). S.S.B., and G.P.G. are CONICET career investigators. M.S. and R.P.M are CONICET doctoral fellows. M.F., A.H.R., and C.A.P. are CONICET technical staff members.

Author Contributions

S.S.B carried out the cloning and protein expression and purification, and designed and performed the *in vitro* experiments and analysed the data. M.F. contributed with protein purification, and preliminary light scattering experiments. K.C.L. performed the cell transfection and immunofluorescence experiments. A.H.R. and S.S.B. designed the FRAP experiments. S.S.B and C.A.P performed the FRAP experiments. R.P.M. contributed with protein purification and protein labelling experiments. S.S.B., M.S., K.G., and G.P.G. participated in data discussions. K.G. designed and supervised the cell culture experiments. G.P.G. conceived and supervised the project. S.S.B. and G.P.G. wrote the manuscript.

Declaration of Interests

The authors declare no competing interest.

Appendix A. Supplementary Data

Supplementary data to this article can be found online at https://doi.org/10.1016/j.jmb.2022.167889.

Received 21 July 2022;
Accepted 7 November 2022;
Available online xxxx

Keywords:
Human papillomavirus;
E2 DNA binding domain;
p53;
LLPS;
Viral protein

References

1. Doorbar, J., Egawa, N., Griffin, H., Kranjec, C., Murakami, I., (2015). Human papillomavirus molecular biology and disease association. *Rev. Med. Virol.* **25** (Suppl 1), 2–23.
2. Schiffman, M., Doorbar, J., Wentzensen, N., de Sanjose, S., Fakhry, C., Monk, B.J., (2016). Carcinogenic human papillomavirus infection. *Nat. Rev. Dis. Primers* **2**, 16086.

3. Basukala, O., Banks, L., (2021). The not-so-good, the bad and the ugly: HPV E5, E6 and E7 oncoproteins in the orchestration of carcinogenesis. *Viruses* **13**
4. McBride, A.A., (2013). The papillomavirus E2 proteins. *Virology* **445**, 57–79.
5. Warburton, A., Della Fera, A.N., McBride, A.A., (2021). Dangerous liaisons: long-term replication with an extrachromosomal HPV genome. *Viruses*, 13.
6. McBride, A.A., (2017). Mechanisms and strategies of papillomavirus replication. *Biol. Chem.* **398**, 919–927.
7. Hegde, R.S., (2002). The papillomavirus E2 proteins: structure, function, and biology. *Annu. Rev. Biophys. Biomol. Struct.* **31**, 343–360.
8. de Prat-Gay, G., Gaston, K., Cicero, D.O., (2008). The papillomavirus E2 DNA binding domain. *Front. Biosci.* **13**, 6006–6021.
9. Levine, A.J., Hu, W., Feng, Z., (2006). The P53 pathway: what questions remain to be explored? *Cell Death Differ.* **13**, 1027–1036.
10. Vogelstein, B., Lane, D., Levine, A.J., (2000). Surfing the p53 network. *Nature* **408**, 307–310.
11. Joerger, A.C., Fersht, A.R., (2008). Structural biology of the tumor suppressor p53. *Annu. Rev. Biochem* **77**, 557–582.
12. Levine, A.J., (2020). P53 and the immune response: 40 years of exploration-A plan for the future. *Int. J. Mol. Sci.*, 21.
13. Robins, H., Alexe, G., Harris, S., Levine, A.J., (2005). The first twenty-five years of p53 research. In: Hainaut, P.W., Wiman, K.G. (Eds.), *25 years of p53 Research*. Springer, Dordrecht, The Netherlands.
14. Scheffner, M., Werness, B.A., Huibregtse, J.M., Levine, A. J., Howley, P.M., (1990). The E6 oncoprotein encoded by human papillomavirus types 16 and 18 promotes the degradation of p53. *Cell* **63**, 1129–1136.
15. Fortunato, E.A., Spector, D.H., (1998). p53 and RPA are sequestered in viral replication centers in the nuclei of cells infected with human cytomegalovirus. *J. Virol.* **72**, 2033–2039.
16. Gannon, J.V., Lane, D.P., (1987). p53 and DNA polymerase alpha compete for binding to SV40 T antigen. *Nature* **329**, 456–458.
17. Konig, C., Roth, J., Dobbelstein, M., (1999). Adenovirus type 5 E4orf3 protein relieves p53 inhibition by E1B–55-kilodalton protein. *J. Virol.* **73**, 2253–2262.
18. Wilcock, D., Lane, D.P., (1991). Localization of p53, retinoblastoma and host replication proteins at sites of viral replication in herpes-infected cells. *Nature* **349**, 429–431.
19. Moody, C.A., Laimins, L.A., (2009). Human papillomaviruses activate the ATM DNA damage pathway for viral genome amplification upon differentiation. *PLoS Pathog.* **5**, e1000605.
20. Massimi, P., Pim, D., Bertoli, C., Bouvard, V., Banks, L., (1999). Interaction between the HPV-16 E2 transcriptional activator and p53. *Oncogene* **18**, 7748–7754.
21. Parish, J.L., Kowalczyk, A., Chen, H.T., Roeder, G.E., Sessions, R., Buckle, M., (2006). E2 proteins from high- and low-risk human papillomavirus types differ in their ability to bind p53 and induce apoptotic cell death. *J. Virol.* **80**, 4580–4590.
22. Brown, C., Kowalczyk, A.M., Taylor, E.R., Morgan, I.M., Gaston, K., (2008). P53 represses human papillomavirus type 16 DNA replication via the viral E2 protein. *Virol. J.* **5**, 5.
23. Banani, S.F., Lee, H.O., Hyman, A.A., Rosen, M.K., (2017). Biomolecular condensates: organizers of cellular biochemistry. *Nat. Rev. Mol. Cell Biol.* **18**, 285–298.
24. Hyman, A.A., Weber, C.A., Julicher, F., (2014). Liquid-liquid phase separation in biology. *Annu. Rev. Cell Dev. Biol.* **30**, 39–58.
25. Shin, Y., Brangwynne, C.P., (2017). Liquid phase condensation in cell physiology and disease. *Science* **357**
26. Kaur, T., Raju, M., Alshareedah, I., Davis, R.B., Potoyan, D.A., Banerjee, P.R., (2021). Sequence-encoded and composition-dependent protein-RNA interactions control multiphasic condensate morphologies. *Nat. Commun.* **12**, 872.
27. Li, P., Banjade, S., Cheng, H.C., Kim, S., Chen, B., Guo, L., (2012). Phase transitions in the assembly of multivalent signalling proteins. *Nature* **483**, 336–340.
28. Kamagata, K., Kanbayashi, S., Honda, M., Itoh, Y., Takahashi, H., Kameda, T., (2020). Liquid-like droplet formation by tumor suppressor p53 induced by multivalent electrostatic interactions between two disordered domains. *Sci. Rep.* **10**, 580.
29. Petronilho, E.C., Pedrote, M.M., Marques, M.A., Passos, Y.M., Mota, M.F., Jakobus, B., (2021). Phase separation of p53 precedes aggregation and is affected by oncogenic mutations and ligands. *Chem. Sci.* **12**, 7334–7349.
30. Lopez, N., Camporeale, G., Salgueiro, M., Borkosky, S.S., Visentin, A., Peralta-Martinez, R., (2021). Deconstructing virus condensation. *PLoS Pathog.* **17**, e1009926.
31. Nikolic, J., Le Bars, R., Lama, Z., Scrima, N., Lagaudriere-Gesbert, C., Gaudin, Y., (2017). Negri bodies are viral factories with properties of liquid organelles. *Nat. Commun.* **8**, 58.
32. Feric, M., Vaidya, N., Harmon, T.S., Mitrea, D.M., Zhu, L., Richardson, T.M., (2016). Coexisting Liquid Phases Underlie Nucleolar Subcompartments. *Cell* **165**, 1686–1697.
33. Riback, J.A., Zhu, L., Ferrolino, M.C., Tolbert, M., Mitrea, D.M., Sanders, D.W., (2020). Composition-dependent thermodynamics of intracellular phase separation. *Nature* **581**, 209–214.
34. Caragliano, E., Bonazza, S., Frascaroli, G., Tang, J., Soh, T.K., Grunewald, K., (2022). Human cytomegalovirus forms phase-separated compartments at viral genomes to facilitate viral replication. *Cell Rep.* **38**, 110469.
35. Hidalgo, P., Pimentel, A., Mojica-Santamaria, D., von Stromberg, K., Hofmann-Sieber, H., Lona-Arrona, C., (2021). Evidence that the adenovirus single-stranded DNA binding protein mediates the assembly of biomolecular condensates to form viral replication compartments. *Viruses*, 13.
36. Charman, M., Weitzman, M.D., (2020). Replication compartments of DNA viruses in the nucleus: location, location, location. *Viruses*, 12.
37. Miciak, J., Bunz, F., (2016). Long story short: p53 mediates innate immunity. *Biochim. Biophys. Acta* **1865**, 220–227.
38. Rivas, C., Aaronson, S.A., Munoz-Fontela, C., (2010). Dual Role of p53 in Innate Antiviral Immunity. *Viruses* **2**, 298–313.
39. Desaintes, C., Goyat, S., Garbay, S., Yaniv, M., Thierry, F., (1999). Papillomavirus E2 induces p53-independent apoptosis in HeLa cells. *Oncogene* **18**, 4538–4545.
40. Fontan, C.T., James, C.D., Prabhakar, A.T., Bristol, M.L., Otoa, R., Wang, X., (2022). A critical role for p53 during the HPV16 life cycle. *Microbiol. Spectr.* **10**, e0068122.

41. Webster, K., Parish, J., Pandya, M., Stern, P.L., Clarke, A. R., Gaston, K., (2000). The human papillomavirus (HPV) 16 E2 protein induces apoptosis in the absence of other HPV proteins and via a p53-dependent pathway. *J. Biol. Chem.* **275**, 87–94.
42. Nikolova, P.V., Henckel, J., Lane, D.P., Fersht, A.R., (1998). Semirational design of active tumor suppressor p53 DNA binding domain with enhanced stability. *Proc. Nat. Acad. Sci. USA* **95**, 14675–14680.
43. Rajagopalan, S., Huang, F., Fersht, A.R., (2011). Single-Molecule characterization of oligomerization kinetics and equilibria of the tumor suppressor p53. *Nucleic Acids Res.* **39**, 2294–2303.
44. Mok, Y.K., de Prat, G.G., Butler, P.J., Bycroft, M., (1996). Equilibrium dissociation and unfolding of the dimeric human papillomavirus strain-16 E2 DNA-binding domain. *Protein Sci. : Publ. Protein Soc.* **5**, 310–319.
45. Alberti, S., Gladfelter, A., Mittag, T., (2019). Considerations and challenges in studying liquid-liquid phase separation and biomolecular condensates. *Cell* **176**, 419–434.
46. Mitrea, D.M., Kriwacki, R.W., (2016). Phase separation in biology; functional organization of a higher order. *Cell Commun. Signal* **14**, 1.
47. Joerger, A.C., Fersht, A.R., (2007). Structure-function-rescue: the diverse nature of common p53 cancer mutants. *Oncogene* **26**, 2226–2242.
48. Sawasdichai, A., Chen, H.T., Abdul Hamid, N., Jayaraman, P.S., Gaston, K., (2010). In situ subcellular fractionation of adherent and non-adherent mammalian cells. *J. Vis. Exp. JoVE*.
49. El-Deiry, W.S., Kern, S.E., Pietenpol, J.A., Kinzler, K.W., Vogelstein, B., (1992). Definition of a consensus binding site for p53. *Nat. Genet.* **1**, 45–49.
50. Ferreiro, D.U., Lima, L.M., Nadra, A.D., Alonso, L.G., Goldbaum, F.A., de Prat-Gay, G., (2000). Distinctive cognate sequence discrimination, bound DNA conformation, and binding modes in the E2 C-terminal domains from prototype human and bovine papillomaviruses. *Biochemistry* **39**, 14692–14701.
51. Banani, S.F., Rice, A.M., Peeples, W.B., Lin, Y., Jain, S., Parker, R., (2016). Compositional control of phase-separated cellular bodies. *Cell* **166**, 651–663.
52. Ferrolino, M.C., Mitrea, D.M., Michael, J.R., Kriwacki, R. W., (2018). Compositional adaptability in NPM1-SURF6 scaffolding networks enabled by dynamic switching of phase separation mechanisms. *Nat. Commun.* **9**, 5064.
53. Ruff, K.M., Dar, F., Pappu, R.V., (2021). Ligand effects on phase separation of multivalent macromolecules. *Proc. Nat. Acad. Sci. USA* **118**
54. Etibor, T.A., Yamauchi, Y., Amorim, M.J., (2021). Liquid biomolecular condensates and viral lifecycles: review and perspectives. *Viruses* **13**
55. Nevers, Q., Albertini, A.A., Lagaudriere-Gesbert, C., Gaudin, Y., (2020). Negri bodies and other virus membrane-less replication compartments. *Biochim. Biophys. Acta* **1867**, 118831.
56. Peng, Q., Wang, L., Qin, Z., Wang, J., Zheng, X., Wei, L., (2020). Phase separation of Epstein-Barr Virus EBNA2 and its coactivator EBNALP controls gene expression. *J. Virol.* **94**
57. Brocca, S., Grandori, R., Longhi, S., Uversky, V., (2020). Liquid-liquid phase separation by intrinsically disordered protein regions of viruses: roles in viral life cycle and control of virus-host interactions. *Int. J. Mol. Sci.*, 21.
58. Seyffert, M., Georgi, F., Tobler, K., Bourqui, L., Anfossi, M., Michaelsen, K., (2021). The HSV-1 transcription factor ICP4 confers liquid-like properties to viral replication compartments. *Int. J. Mol. Sci.*, 22.
59. Caragliano, E., Brune, W., Bosse, J.B., (2022). Herpesvirus replication compartments: dynamic biomolecular condensates? *Viruses*, 14.
60. Metrick, C.M., Koenigsberg, A.L., Heldwein, E.E., (2020). Conserved outer tegument component UL11 from herpes simplex virus 1 is an intrinsically disordered, RNA-binding protein. *MBio*, 11.
61. Vladimirova, O., De Leo, A., Deng, Z., Wiedmer, A., Hayden, J., Lieberman, P.M., (2021). Phase separation and DAXX redistribution contribute to LANA nuclear body and KSHV genome dynamics during latency and reactivation. *PLoS Pathog.* **17**, e1009231.
62. De Leo, A., Calderon, A., Lieberman, P.M., (2020). Control of viral latency by episome maintenance proteins. *Trends Microbiol.* **28**, 150–162.
63. Cai, Q.L., Knight, J.S., Verma, S.C., Zald, P., Robertson, E. S., (2006). EC5S ubiquitin complex is recruited by KSHV latent antigen LANA for degradation of the VHL and p53 tumor suppressors. *PLoS Pathog.* **2**, e116.
64. Khurana, S., Markowitz, T.E., Kabat, J., McBride, A.A., (2021). Spatial and functional organization of human papillomavirus replication foci in the productive stage of infection. *mBio*, e0268421.
65. Sakakibara, N., Mitra, R., McBride, A.A., (2011). The papillomavirus E1 helicase activates a cellular DNA damage response in viral replication foci. *J. Virol.* **85**, 8981–8995.
66. Day, P.M., Roden, R.B., Lowy, D.R., Schiller, J.T., (1998). The papillomavirus minor capsid protein, L2, induces localization of the major capsid protein, L1, and the viral transcription/replication protein, E2, to PML oncogenic domains. *J. Virol.* **72**, 142–150.
67. Kilic, S., Lezaja, A., Gatti, M., Bianco, E., Michelena, J., Imhof, R., (2019). Phase separation of 53BP1 determines liquid-like behavior of DNA repair compartments. *EMBO J.* **38**, e101379.
68. Krois, A.S., Ferreon, J.C., Martinez-Yamout, M.A., Dyson, H.J., Wright, P.E., (2016). Recognition of the disordered p53 transactivation domain by the transcriptional adapter zinc finger domains of CREB-binding protein. *Proc. Nat. Acad. Sci. USA* **113**, E1853–E1862.
69. Sun, X., Dyson, H.J., Wright, P.E., (2021). A phosphorylation-dependent switch in the disordered p53 transactivation domain regulates DNA binding. *Proc. Nat. Acad. Sci. USA* **118**
70. Smal, C., Wetzler, D.E., Dantur, K.I., Chemes, L.B., Garcia-Alai, M.M., Dellarole, M., (2009). The human papillomavirus E7–E2 interaction mechanism in vitro reveals a finely tuned system for modulating available E7 and E2 proteins. *Biochemistry* **48**, 11939–11949.
71. Alshareedah, I., Kaur, T., Banerjee, P.R., (2021). Methods for characterizing the material properties of biomolecular condensates. *Methods Enzymol.* **646**, 143–183.